

# OPTICAL TO X-RAYS SUPERNOVAE LIGHT CURVES FOLLOWING SHOCK BREAKOUT THROUGH A THICK WIND

GILAD SVIRSKI<sup>1</sup>, EHUD NAKAR<sup>1</sup> AND RE'EM SARI<sup>2</sup>

1. Raymond and Beverly Sackler School of Physics & Astronomy, Tel Aviv University, Tel Aviv 69978, Israel
2. Racah Institute for Physics, The Hebrew University, Jerusalem 91904, Israel

*Draft version November 19, 2018*

## Abstract

Recent supernovae (SNe) observations have motivated renewed interest in SN shock breakouts from stars surrounded by thick winds. In such events the interaction with the wind powers the observed luminosity, and predictions include observable hard X-rays. Wind breakouts on timescales of a day or longer are currently the most probable for detection. Here we study the signal that follows such events. We start from the breakout of the radiation mediated shock, finding that the breakout temperature can vary significantly from one event to another ( $10^4 - 5 \times 10^6$  K) due to possible deviation from thermal equilibrium. In general, events with longer breakout pulse duration,  $t_{bo}$ , are softer. We follow the observed radiation through the evolution of the collisionless shock which forms after the breakout of the radiation mediated shock. We restrict the study of the collisionless shock evolution to cases where the breakout itself is in thermal equilibrium, peaking in optical/UV. In these cases the post-breakout emission contains two spectral components - soft (optical/UV) and hard (X-rays and possibly soft  $\gamma$ -rays). Right after the breakout pulse X-rays are strongly suppressed, and they carry only a small fraction of the total luminosity. The hard component becomes harder and its luminosity rises quickly afterwards, gaining dominance at  $\sim 10 - 50 t_{bo}$ . The ratio of the peak optical/UV to the peak X-ray luminosity depends mostly on the breakout time. In early breakouts ( $t_{bo} \lesssim 20$  d for typical parameters) they are comparable, while in late breakouts ( $t_{bo} \gtrsim 80$  d for typical parameters) the X-rays become dominant only after the total luminosity has dropped significantly. In terms of prospects for X-ray and soft gamma-ray detections, it is best to observe 100-500 days after explosions with breakout timescales between a week and a month.

## 1. INTRODUCTION

The breakout of a supernova (SN) shock through the stellar surface has been an active field of analytic and numerical research for several decades (e.g. Colgate 1974, Weaver 1976, Falk 1978, Klein & Chevalier 1978, Imshennik et al. 1981, Ensmann & Burrows 1992, Matzner & McKee 1999). Recent advancement of observational facilities led to the discovery of several shock breakout candidates (e.g., Campana et al. 2006; Soderberg et al. 2008; Gezari et al. 2008; Schawinski et al. 2008; Modjaz et al. 2009; Ofek et al. 2010; Gezari et al. 2010; Arcavi et al. 2011) which motivated a revisit of the theory of shock breakout (e.g., Chevalier & Fransson 2008; Katz et al. 2010; Piro et al. 2010; Nakar & Sari 2010; Murase et al. 2011; Katz et al. 2011a; Rabinak & Waxman 2011; Couch et al. 2011; Nakar & Sari 2011; Chevalier & Irwin 2011; Balberg & Loeb 2011; Moriya & Tominaga 2011).

The main observational challenge posed by shock breakouts from stellar surfaces is their short duration (no more than an hour even in the case of a red supergiant). However, in some cases massive mass loss prior to the SN explosion can extend the breakout signal, facilitating its detection. Ofek et al. (2010) and Chevalier & Irwin (2011) show that a breakout through a thick wind may occasionally extend long enough to account for the complete SN luminosity light curve, and suggest that at least some type II<sub>n</sub> SNe are in fact powered by such breakouts.

When a star goes through a SN explosion, a radiation mediated shock (RMS) is driven through its enve-

lope, accelerating through the sharp density drop near the stellar edge (Sakurai 1960). If the star is not surrounded by a thick wind then the shock breaks out of the stellar surface, producing an intense short pulse of UV-X-ray photons. If, on the other hand, the star is surrounded by a wind with an optical depth between the stellar edge and the observer  $> c/v$ , where  $c$  is the speed of light and  $v$  is the shock speed, then the shock continues into the wind without releasing photons to the observer. At this point the shock starts decelerating and a reverse-forward shock structure is formed. The reverse shock is driven into the SN ejecta, which is characterized by a sharp rise in the amount of energy that is carried by slower moving material. The reverse shock is driving an increasing amount of energy into the shocked region, which keeps accumulating until the wind optical depth drops to  $c/v$ . Beyond this point the wind cannot contain anymore the radiation mediated forward shock and the shock is breaking out of the wind, releasing all its energy as an intense pulse. This pulse can contain much more energy than a wind-less breakout, over timescales that are much longer. The general properties of a wind breakout were recently discussed by Ofek et al. (2010) and Chevalier & Irwin (2011), who find the pulse luminosity and temperature assuming thermal equilibrium, and by Balberg & Loeb (2011) who also show how the progenitor mass and explosion energy can be constrained by the pulse observational properties.

If the wind density does not fall abruptly, the energy behind the shock keeps growing after breakout, and the

characteristic evolution of the resultant signal supplies an important observational probe for the interaction of the forward shock with the wind. Katz et al. (2011b) showed that if the breakout of the RMS occurs within the wind, i.e. the matter consisting the breakout layer is spread over a scale comparable to the breakout radius rather than being concentrated within a thin layer, then a collisionless shock is bound to develop and replace the RMS in accelerating the matter ahead. This collisionless shock heats the immediate post-shock electrons to  $k_B T_e \sim 60$  keV (Katz et al. 2011b; Murase et al. 2011), where  $T_e$  is the electron temperature and  $k_B$  is the Boltzmann constant. The cooling processes of these electrons affect the observed temperature (and possibly the luminosity evolution), which is further influenced by the interplay between photons and electrons along the photons diffusion path to the observer.

Here we examine the evolution of the luminosity and the observed temperature at and following a wind shock breakout. We consider only breakouts through a wind that is dense enough to produce a breakout pulse lasting days or longer, which are easier to detect. We restrict the discussion on the observed radiation during the collisionless shock evolution to scenarios where the unshocked electrons ahead of the shock and the radiation that diffuses through them on its way to the observer, are in thermal equilibrium. This condition implies shock velocities  $\lesssim 10^4$  km/s, where the exact limiting velocity can vary with the gas metallicity. Finally, we consider only cases where the shocks are cooling fast during the entire evolution, i.e., the shock heated plasma cool within a dynamical time. This condition is satisfied for regular SNe parameters. We pay attention to hydrodynamic, diffusion and cooling timescales involved, and show that the breakout timescale is the most dominant parameter in determining the post-breakout evolution. We map the different types of post breakout behaviors and describe their light curves and spectra evolution.

As this work was near completion, Chevalier & Irwin (2012) submitted a paper, presenting some of the conclusions derived below in the context of explaining the low X-ray luminosity of SN 2006gy, observed by *Chandra* at an age of 3-4 months. The low luminosity is explained as the result of three factors: two, which are discussed in details below, are the domination of inverse Compton over free-free emission in cooling the hot post-shock electrons, and the energy degradation of the hard free-free emitted photons over the diffusion path. The third is photoabsorption of soft X-rays by partially ionized pre-shock gas. This latter process is not considered in this work.

## 2. HYDRODYNAMIC EVOLUTION AND CHARACTERISTIC SCALES

We consider the interaction of SN ejecta with a dense stellar wind that follows a standard profile  $\rho_w = Dr^{-2}$ , where  $D$  is a constant and  $r$  is the radius. This wind profile implies  $\tau \propto r^{-1}$ , where  $\tau$  is the optical depth of the wind at the location of the shock. It also implies a photon diffusion time scale to the observer, that is independent of the radius (up to a logarithmic factor),  $t_{diff} \sim \kappa D/c$ , where  $\kappa$  is the cross section per unit of mass (throughout the paper we assume that the gas which dominates the optical depth is fully ionized, and take  $\kappa = 0.34$  cm<sup>2</sup>g<sup>-1</sup>).

During the interaction, a forward shock is driven into the wind while a reverse shock is driven into the ejecta. Chevalier (1982) derives a self similar solution of the forward-reverse shock structure, assuming that both the ejecta and the wind density profiles are power-laws:

$$r(t) \propto t^{\frac{n-3}{n-2}} \quad (1)$$

for  $\rho_w \propto r^{-2}$  and  $\rho_{ej} \propto v^{-n}$ . The ejecta density profile through which the reverse shock is propagating is determined by the SN shock that crosses the stellar envelope. The density profile of the fastest moving ejecta can be approximated by a power-law with an index<sup>1</sup>  $n \approx 10 - 12$  for all progenitor types. The ejecta density profile flattens towards the slower layers which contain most of the ejecta mass and energy, (e.g. Matzner & McKee 1999). As the reverse shock approaches these layers the evolution is no longer strictly self-similar, but it can be approximated by the self-similar solution using  $n = 7$  (e.g., Chevalier & Irwin 2011, 2012). Given that during the reverse-forward shock interaction phase  $n \gtrsim 7$  we hereafter approximate  $\frac{n-3}{n-2} \approx 1$  during this phase. Finally, once the reverse shock ends crossing the ejecta only the forward shock remains, entering a Sedov-Taylor phase if the shock is adiabatic or a snowplow phase if it is radiative.

The density power-law indices of the ejecta and the wind are set by the pre-explosion stellar evolution and are not expected to vary much between various SN progenitors. The difference in the hydrodynamical evolution during the forward-reverse shock phase between various SNe is set by the two normalization factors of these density profiles. These could be determined by two observables such as the duration of the breakout pulse,  $t_{bo}$ , which is set by the wind density only,  $t_{bo} \sim \kappa D/c$  (Ofek et al. 2010; Chevalier & Irwin 2011; Balberg & Loeb 2011), and the breakout luminosity  $L_{bo}$ . Below we present the evolution during the interaction phase using  $t_{bo}$  and the shock breakout velocity  $v_{bo}$ , (instead of  $L_{bo}$ ) which is related to the observables via  $v_{bo} = \left(\frac{\kappa}{4\pi c} L_{bo} t_{bo}^{-1}\right)^{1/3}$  (Balberg & Loeb 2011). The evolution after the interaction phase ends depends on three parameters and we present it using  $t_{bo}$ , the total explosion energy,  $E$ , and ejecta mass,  $M_{ej}$ .

The breakout from the wind takes place once  $\tau_{bo} \approx c/v_{bo}$ , where  $\tau_{bo}$  is the wind optical depth to the observer at the breakout radius. This sets the mass swept by the shock at the time of the breakout:

$$m_{bo} \approx \frac{4\pi c}{\kappa} v_{bo} t_{bo}^2 \approx 5 \times 10^{-3} M_{\odot} v_{bo,9} t_{bo,d}^2, \quad (2)$$

where  $v_{bo,9} = \frac{v_{bo}}{10^9 \text{ cm/s}}$  and  $t_{bo,d} = \frac{t_{bo}}{1 \text{ day}}$ . During the ejecta-wind interaction the wind mass collected by the forward shock is comparable to the ejecta mass collected by the reverse shock. Therefore,  $v_{bo}$  can be found using the velocity profile of an ejecta released by a SN explosion (e.g., from Nakar & Sari 2010; hereafter NS10), and requiring that a wind mass collected

<sup>1</sup> The mass profile for  $m \ll M_{ej}$  is  $m \propto v^{-\frac{\bar{n}+1}{0.19\bar{n}}}$  where  $\bar{n}$  (not to be confused with  $n$ ) is the power-law index of the pre-explosion stellar density profile near the edge. This profile translates, under free expansion, to  $\rho_{ej} \propto t^{-3} v^{-3-\frac{\bar{n}+1}{0.19\bar{n}}}$ , or  $n \approx 10$  for a radiative envelope and  $n \approx 12$  for a convective one

by the forward shock until the breakout,  $m_{bo}$ , is accelerated to  $v_{bo}$  by the explosion. Equations A2 and A4 from NS10 provide the ejecta velocity profile  $v(m) \approx 3 \cdot 10^8 \text{ cm/s} \left( \frac{m}{M_{ej}} \right)^{-\frac{0.19\tilde{n}}{\tilde{n}+1}} \left( \frac{E_{51}}{M_{10}} \right)^{1/2}$ , where  $M_{10} = \frac{M_{ej}}{10M_{\odot}}$ ,  $E_{51} = \frac{E}{10^{51} \text{ erg}}$  and  $\tilde{n}$  (not to be confused with  $n$ ) is the power-law index of the pre-explosion stellar density profile near the edge ( $\tilde{n} = 3$  for a fully radiative envelope and  $\tilde{n} = 1.5$  for a fully convective one). Plugging Equation 2 into this velocity profile we find:

$$v_{bo} \approx 10^9 \text{ cm/s} M_{10}^{-0.35} E_{51}^{0.45} t_{bo,d}^{-0.2}, \quad (3)$$

where the dependence on  $\tilde{n}$  is weak. This equation is applicable until  $m_{bo} = M_{ej}$ . It implies that for typical SNe (e.g., not extremely high or low  $E_{51}/M_{10}$ ) and in the range of  $t_{bo}$  that we consider ( $\gtrsim 1$  day) the breakout velocity does not vary much. Thus, we consider here only a narrow range of  $v_{bo,9} \approx 0.3 - 1.5$ . The upper limit of this range ensures that shocks that follow breakouts with timescales of days or longer remain fast cooling (i.e., the shock heated plasma radiate its energy within a dynamical time) at all times (see section 3.4). When studying the post breakout evolution we further limit the shock velocity by studying scenarios where the unshocked wind electrons maintain thermal equilibrium with the diffusing radiation, which typically implies  $v_{bo,9} \lesssim 1$ . Note that since  $v(m)$  is independent of the progenitor radius (the radius determines only the maximal ejecta velocity), Equation 3 is independent of the radius. Since Equation 3 is also only weakly sensitive to the exact density profile near the stellar edge, it is applicable to red and blue supergiant as well as Wolf-Rayet progenitors. Thus, if the shock is breaking out from a thick wind, the wind density is the parameter that affects the observed radiation the most, and the progenitor type cannot be identified based on the light curve alone.

An important time scale, which affects the hydrodynamic evolution, is the time at which the wind mass collected by the forward shock,  $m$ , is comparable to the total ejecta mass. At that point the reverse shock stops playing a role and the forward shock is slowing down rapidly. The deceleration rate depends on whether the shock is adiabatic, or a significant fraction of the post-shock internal energy is radiated away. If it is adiabatic then the evolution follows the Sedov-Taylor self similar solution. If, on the other hand, all the internal energy behind the shock is radiated within a dynamical time scale, then the shock enters the so called snowplow phase. We consider only fast cooling shocks, which are in the snowplow regime when  $m \geq M_{ej}$  and  $t > t_{bo}$ .

Next we find the time of transition to snowplow,  $t_{SP}$ , in case that  $t_{bo} < t_{SP}$ . Equation 1 for  $r(t)$  can also be applied for the snowplow phase using  $n = 4$  (the Sedov-Taylor phase matches  $n = 5$ )<sup>2</sup>. Therefore, in case that  $t_{bo} < t_{SP}$  the swept mass after breakout accumulates as

$$m(t) \approx \begin{cases} m_{bo} \frac{t}{t_{bo}} & t_{bo} < t < t_{SP} \\ M_{ej} \left( \frac{t}{t_{SP}} \right)^{1/2} & t_{SP} < t \end{cases} \quad (4)$$

<sup>2</sup> Note that using  $n = 4$  in Equation 1 provides the correct evolution in the snowplow regime, although Chevalier (1982) derived it for the interaction phase only.

Since the snowplow regime begins once  $m = M_{ej}$ , it follows from Equation 2 that if  $t_{bo} \lesssim 80 M_{10}^{0.75} E_{51}^{-0.25}$  d then  $t_{bo} < t_{SP}$ , where we approximate the shock velocity at the transition to the snowplow phase with  $\sqrt{2E/M_{ej}}$ . The transition time to snowplow phase occurs then at

$$t_{SP} = 7 \times 10^3 t_{bo,d}^{-1} M_{10}^{3/2} E_{51}^{-1/2} \text{ d} \quad (5)$$

If  $m = M_{ej}$  before breakout, then the evolution follows a Sedov-Taylor expansion prior to breakout and assumes a snowplow evolution afterwards. In such case we say that  $t_{SP} < t_{bo}$  and the mass behind the forward shock accumulates as

$$m(t) \approx m_{bo} \left( \frac{t}{t_{bo}} \right)^{1/2} \quad t_{SP} < t_{bo} < t \quad (6)$$

### 3. TEMPERATURE AND LUMINOSITY EVOLUTION

#### 3.1. Bolometric luminosity

The bolometric luminosity of a fast cooling shock is  $L \approx 2\pi r^2 \rho v^3 \propto v^3 \propto t^{-\frac{3}{n-2}}$ . Therefore, if the breakout takes place before  $t_{SP}$  then

$$L(t) \sim \begin{cases} 5 \times 10^{43} t_{bo,d} v_{bo,9}^3 \left( \frac{t}{t_{bo}} \right)^{-0.3} \frac{\text{erg}}{\text{s}} & t_{bo} < t \ll t_{SP} \\ 2 \times 10^{42} t_{bo,d} M_{10}^{-3/2} E_{51}^{3/2} \left( \frac{t}{t_{SP}} \right)^{-1.5} \frac{\text{erg}}{\text{s}} & t_{SP} \lesssim t \end{cases} \quad (7)$$

while if  $t_{bo} > t_{SP}$  then

$$L(t) \sim 5 \times 10^{43} t_{bo,d} v_{bo,9}^3 \left( \frac{t}{t_{bo}} \right)^{-1.5} \frac{\text{erg}}{\text{s}} ; \quad t_{SP} < t_{bo} < t. \quad (8)$$

Note that once the radiation escape time becomes shorter than the dynamical time (i.e., after breakout), then as long as the shock is cooling fast, the bolometric luminosity is simply the kinetic energy flux through the shock. In contrast to regular SNe, it is independent of the gas opacity, and thus insensitive to processes such as recombination or to the gas metallicity.

#### 3.2. Breakout temperature

The first signal to be observed is the breakout pulse, releasing over a diffusion time  $t_{diff} \sim t_{bo}$  the energy accumulated during the interaction with the wind prior to the breakout. The pre-breakout forward shock is radiation mediated, but the photons that mediate the shock and dominate the energy density behind the shock cannot escape before breakout. As the breakout occurs, these photons start leaking towards the observer and their observed temperature is set by their interaction with the unshocked wind through which they diffuse.

The unshocked wind is heated by the diffusing radiation. It produces photons, mostly by free-free, which share energy with the diffusing radiation. The breakout temperature is therefore set by the ability of the unshocked wind to produce photons over the radiation diffusion time. The radiation energy density at any point along the diffusion path is  $\epsilon_{rad} \sim \frac{Lr}{cr^2}$ . We define  $T_{BB} \equiv (\epsilon_{rad}/a)^{1/4}$ , where  $a$  is the radiation constant. If photons are abundant enough behind the shock and the radiation is in thermal equilibrium, then the photon

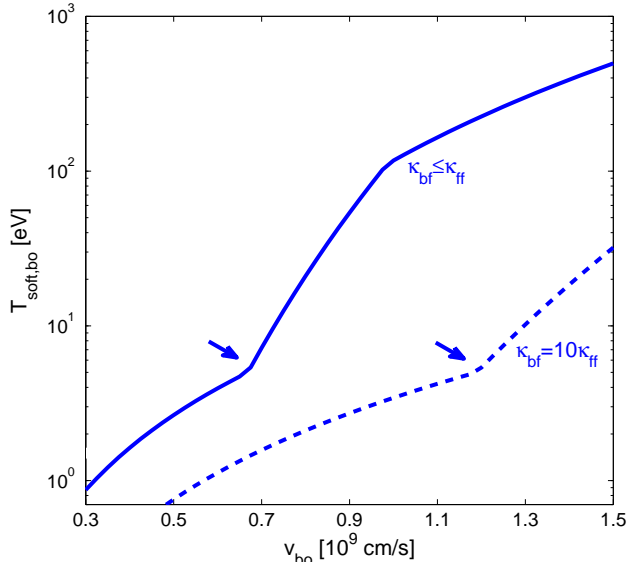


FIG. 1.— The observed breakout temperature as a function of the breakout velocity for  $t_{bo} = 20$  d, demonstrating the strong effect of deviation from thermal equilibrium on the observed temperature. Departure from equilibrium is indicated by arrows. The solid line assumes photons are produced solely by free-free emission (low metallicity). The relatively small range of relevant velocities  $0.3 < v_{bo,9} < 1.5$  corresponds to a range spanning over 2.5 orders of magnitude in temperature,  $10^4 K < T_{bo} < 5 \times 10^6 K$ . The dashed line assumes a bound-free opacity ten times that of free-free, resulting in departure from thermal equilibrium at higher velocity and lower breakout temperatures. The latter is because thermal equilibrium is kept farther ahead of the shock, thereby reducing the observed temperature, although the shock temperature is independent of the opacity.

temperature at the shock is  $T_{BB}$ . The observer is seeing, however, a lower temperature. The reason is that thermal equilibrium is also kept at radii that are larger than the shock radius and  $\tau$  is lower, where the radiation energy density is lower. Thus, the observed temperature is set by the radiation energy density at the largest radius at which thermal equilibrium is kept. If, in contrast, the photons at the shock are out of thermal equilibrium, then the observed temperature can be much higher than  $T_{BB}$ , and is set by the number of photons that are generated over the diffusion time. This process is the same one as in the case of a shock breakout from a stellar surface where no wind is present, and is discussed in length in Katz et al. (2010) and NS10.

Assuming that photons and electrons in the unshocked wind have the same temperature, the observed temperature can be determined using the coupling coefficient  $\eta \equiv 5 \times 10^{-36} T_{BB}^{3.5} \rho^{-2} t_{diff}^{-1}$  defined in NS10, where all quantities are in c.g.s. units. Here  $\eta$  is the ratio of the photon density needed to maintain thermal equilibrium to the photons produced per unit of volume during the diffusion time, assuming that the electrons' temperature is  $T_{BB}$ . This value of  $\eta$  assumes that free-free emission dominates photon production. If bound-free opacity for  $T_{BB}$  photons,  $\kappa_{bf}$ , is higher than free-free opacity,  $\kappa_{ff}$ , then  $\eta$  is lower by the factor  $\kappa_{bf}/\kappa_{ff}$  (see discussion in NS10). When the value of  $\eta$  at the shock radius is  $\eta_s < 1$ , the radiation is in thermal equilibrium and the temper-

ature is set by the electrons at the radius where<sup>3</sup>  $\eta = 1$ .

At breakout,  $aT_{BB}^4/3 = (6/7)\rho_w v_{bo}^2$ , implying

$$T_{BB,bo} = \left( \frac{18c}{7\kappa a t_{bo}} \right)^{1/4} \approx 10^5 t_{bo,d}^{-1/4} \text{ K}, \quad (9)$$

and yielding<sup>4</sup>

$$\eta_{bo} \approx 5 \left( 1 + \frac{\kappa_{bf}}{\kappa_{ff}} \right)^{-1} v_{bo,9}^4 t_{bo,d}^{1/8}, \quad (10)$$

where free-free is assumed to be the main source of photons, (and absorption opacity). At any given time  $\eta \propto r^{11/8}$ , implying that if  $\eta_{bo} \ll 1$ , then the observed temperature of the breakout pulse is  $T_{BB,bo} \eta_{bo}^{6/11}$ , yielding an observed breakout temperature

$$T_{bo,obs}(\eta_{bo} < 1) \approx 2 \times 10^4 \left( 1 + \frac{\kappa_{bf}}{\kappa_{ff}} \right)^{-\frac{6}{11}} \left( \frac{v_{bo}}{3000 \frac{\text{km}}{\text{s}}} \right)^{2.2} t_{bo,d}^{-0.2} \text{ K}. \quad (11)$$

In contrast, when  $\eta_{bo} \gg 1$ , then the observed breakout temperature is much higher than  $T_{BB}$  and is given by  $T_{BB,bo} \eta_{bo}^2 \xi^{-2}$  (Equation 13 in NS10). This equation is implicit since the factor  $\xi$  depends on  $T_{BB,bo}$ .  $\xi$  is a logarithmic factor which accounts for the contribution of inverse Compton in bringing the temperature closer to thermal equilibrium ( $\xi$  always  $\geq 1$ ). It is discussed in length in NS10 and its value is  $\sim 1$  at low temperatures ( $\lesssim 10^6$  K) and  $\sim 10$  at high temperatures ( $\gtrsim 10^7$  K). In the scenario that we discuss here the calculation of  $\xi$  is slightly modified compared to the one described in NS10, where the softest photon that is thermally coupled to the electrons is set by the requirement that its energy is doubled before it is absorbed by free-free (see their Equation 11). Here, where the optical depth of the wind can be low enough, the limiting factor may become instead the low Compton y-parameter of the wind. In our calculations below we use both requirements (high enough y-parameter and no free-free absorption) to find the softest photons that are coupled by IC to the electrons.

Figure 1 depicts the observed breakout temperature as a function of the breakout velocity for  $t_{bo} = 20$  d. The solid line describes a wind composition such that photons production (and absorption) is dominated by free-free emission. In that case the critical breakout velocity, above which thermal equilibrium cannot be maintained, is  $\approx 7000 \text{ km s}^{-1}$ . It is evident that  $T_{bo,obs}$  depends strongly on deviation from thermal equilibrium,

<sup>3</sup> We assume here that the Thompson cross section is larger than the free-free absorption cross section and that  $\tau > 1$ . This is true during the breakout and later while the soft component is dominant

<sup>4</sup> Note that calculating  $\eta$  for the configuration of a wind breakout is slightly different than in the steady state planar case discussed by Weaver (1976) and Katz et al. (2010). The reason is that in a steady state shock photons that are diffusing from the downstream back to the shock, over the shock crossing time, are produced by a mass that is larger by the shock compression ratio, 7 in this case, than the mass in the shock transition layer. In the case of a wind breakout the mass behind the shock is comparable to the mass in the shock transition layer at the time of breakout. Therefore  $\eta_{bo}$  is larger by a factor of  $\approx 7$  compared to the one that is calculated for the same shock velocity in steady state. As a result the radiation behind the wind breakout shock falls out of thermal equilibrium already when the shock exceeds  $7000 \text{ km s}^{-1}$  (for  $\kappa_{bf} < \kappa_{ff}$ ) instead of  $15,000 \text{ km s}^{-1}$  in the steady state case.

rising by more than an order of magnitude when  $v_{bo}$  is increased by a factor of 2. Thus, for  $v_{bo,9} = 0.3$  we find  $T_{bo,obs} \approx 10^4$  K while if  $v_{bo,9} = 1.5$  then  $T_{bo,obs} \approx 5 \times 10^6$  K. The effect of high metallicity is demonstrated by the dashed line in Figure 1, describing the observed breakout temperatures in case that  $\kappa_{bf}/\kappa_{ff} = 10$  (and  $\eta_{bo}$  is smaller by that factor). Evidently, a higher metallicity implies a thermal equilibrium also at higher velocities. Note, that  $T_{bo,obs}$  at which thermal equilibrium breaks is almost independent of the exact opacity ( $5 \times 10^4$  K in Figure 1). It also depends weakly on  $t_{bo}$  and is always  $< 10^5$  K. Since the velocity range that we consider here is exactly at the point where thermal equilibrium is marginal, we expect some of the breakouts in this range to be in equilibrium with  $T_{bo,obs} \sim 10^4 - 10^5$  K, therefore bright in optical/UV, and some to be out of thermal equilibrium with  $T_{bo,obs} > 10^6$  K, bright in soft X-rays, but faint in optical.

### 3.3. Post breakout evolution

Following breakout, the collisionless shock that develops heats protons to high temperatures. The protons then transfer heat to electrons, which are cooled by radiation. The balance between the electrons heating and cooling rates sets the electron temperature, during the post-shock cooling process (Katz et al. 2011b; Murase et al. 2011). The breakout balance temperature is<sup>5</sup>  $\sim 60$  keV, independent of the shock velocity. If the protons temperature,  $k_B T_p \approx \frac{3}{16} m_p v^2 \approx 200 v_9^2$  keV where  $m_p$  is the proton mass, is lower than the implied balance temperature, then  $T_e \sim T_p$ . Thus

$$k_B T_{e,bo} \sim \min [200 v_{bo,9}^2, 60] \text{ keV.} \quad (12)$$

It is straight forward to show that after breakout  $T_e$  approaches  $T_p$  (if they were not similar already at breakout). Now, since we consider  $v_{bo,9} = 0.3 - 1.5$ , the electron and proton temperatures are not very different already during the breakout, and at  $t < t_{SP}$  the proton and electron temperatures are approximately constant. At  $t > t_{SP}$  the proton temperature drops, and  $T_e$  follows it. Therefore, the electron temperature can be approximated as

$$k_B T_e(t) \sim \begin{cases} 60 \text{ keV} & t < t_{SP} \\ 20 E_{51} M_{10}^{-1} \left(\frac{t}{t_{SP}}\right)^{-1} \text{ keV} & t > t_{SP} \end{cases}. \quad (13)$$

While the electrons behind the collisionless shock are hot, the observed radiation at the breakout, and soon after it, is much softer (Chevalier & Irwin 2012). The reason is that energy of the shocked electrons is deposited into photons that diffuse through the optically thick colder gas that lies ahead of the shock. During the

<sup>5</sup> This equation assumes that the shock does not couple the electrons to the protons and that the electron heating is by Coulomb interactions. In this case the electrons Coulomb heating and radiative cooling are both proportional to protons kinetic energy and the resultant electrons balance temperature is independent of the shock velocity. If instead the shock couples the electrons to the protons then electrons are heated by the shock to  $T_p$  and then cool down until the radiative cooling and Coulomb heating is balanced. Since the difference between  $T_p$  and  $T_e$  is not large under any of the two scenarios their predictions for the observed signature are similar.

diffusion, the temperature of hard photons is reduced via Compton scattering on the unshocked, lower temperature, wind electrons. Moreover, the outgoing radiation heats the unshocked gas along the diffusion path, which in turn produces photons via free-free and bound-free emission. In the case that we consider here the gas ahead of the shock is in thermal equilibrium and its temperature is in the optical-UV range. The generated optical-UV photons dominate the radiation energy density and are the main cooling source, via inverse Compton (IC) of the hot shocked electrons. Thus, the energy in hard photons, which are emitted by free-free emission of the hot shocked electrons, is suppressed farther by the free-free to IC cooling rate ratio.

Hence, if the electrons of the unshocked wind maintain thermal equilibrium with the diffusing radiation (not to be confused with the hot post-shock electrons that are always out of thermal equilibrium) the observed spectrum which follows the breakout pulse will have two distinct components, a soft one and a hard one. Photons of the softer component, which dominates the luminosity at early times, are produced by the unshocked electrons and their main energy source is IC over the hot shocked electrons. The hot electrons themselves radiate hard free-free photons at  $T_e$ . The observed temperature of these hard photons is determined by the energy loss of a single photon while it diffuses out of the wind and their fraction of the total luminosity is set by the product of this energy loss and the free-free to IC cooling rate ratio. Below we describe the temperature evolution of the soft component,  $T_{soft}$ , and the temperature and luminosity of the hard component,  $T_{hard}$  and  $L_{hard}$ , while  $T_{soft}$  is in thermal equilibrium.

#### 3.3.1. Soft component

The shock-heated electrons and protons are confined to a narrow layer behind the shock. Although they are the source of the observed luminosity, they do not necessarily set the typical photon temperature. This temperature is set during the diffusion of the photons towards the observer through the unshocked wind, as long as it is optically thick<sup>6</sup>.

The electrons of the unshocked wind are much colder than the  $\sim 60$  keV electrons immediately behind the shock. These unshocked electrons are heated by the diffusing radiation, and they produce photons which share energy with the diffusing radiation. During the early evolution after the breakout, the major part of the  $\sim 60$  keV electrons layer cooling occurs as photons produced by the unshocked electrons diffuse back into the hot electrons layer behind the shock, and heat up by inverse Compton over this hot layer. These upscattered photons also serve during this stage as the main heating source of the

<sup>6</sup> Fast cooling dictates that the shocked plasma is cooling, forming a dense cold layer behind the hot shock heated plasma. This cold layer does not affect the observed soft component. The reason is that after the breakout the photons escape on a time that is shorter than the dynamical time, and therefore the energy density behind the shock is not dominated by radiation. Since the shock is radiative the shocked plasma is compressed to keep the pressure balance and once free-free cooling becomes dominant, its cooling rate increases with the compression and a run-away cooling decouples the plasma temperature from the rest of the system, preventing it from contributing a significant number of photons to the radiation field that cools the shock heated plasma.

unshocked electrons, through absorption of photons with similar temperature, and possibly also through Compton collisions with photons upscattered to  $m_e c^2/\tau^2$ , where Compton losses are substantial. The balance between the heating and the cooling of the unshocked electrons determines their temperature.

If unshocked electrons are able to produce a sufficient amount of photons during the available diffusion time, then the diffusing radiation is in thermal equilibrium. The condition for thermal equilibrium during the post-breakout evolution is similar to that during the breakout, namely  $\eta < 1$ . Thermal equilibrium also implies that each photon with  $T \sim T_{BB}$  is absorbed at least once during its diffusion through the unshocked electrons. This ensures that the unshocked electrons and the diffusing photons share a single temperature and the observed temperature is simply  $T_{BB}$  at the outermost layer that can maintain thermal equilibrium, namely the layer where  $\eta = 1$ . At breakout, the blackbody temperature of the diffusing radiation just ahead of the shock is  $T_{BB,s} = T_{BB,bo}$ , and the thermal coupling coefficient of the electrons at this location is  $\eta_s = \eta_{bo}$ . Following the breakout  $T_{BB}$  and  $\eta_s$  (both measured at the shock radius) evolve as

$$T_{BB,s}(t) \propto \left(\frac{L\tau}{r^2}\right)^{1/4} \propto t^{-3/4}, \quad (14)$$

independent of  $n$ , and

$$\eta_s(t) \propto \frac{T_{BB,s}^{3.5}}{\rho^2} \propto T_{BB}^{3.5} r^4 \propto \begin{cases} t^1 & n = 12 \\ t^{0.6} & n = 7 \\ t^{-0.6} & n = 4 \end{cases}. \quad (15)$$

The evolution of the observed soft component temperature ( $T_{BB}$  where  $\eta = 1$ ) while thermal equilibrium is maintained is therefore:

$$T_{soft}(t, \eta_s < 1) \propto T_{BB,s} \eta_s^{6/11} \propto \begin{cases} t^{-0.2} & n = 12 \\ t^{-0.45} & n = 7 \\ t^{-1.1} & n = 4 \end{cases}. \quad (16)$$

Thus, while  $\eta_s < 1$ , the observed temperature decreases slowly at  $t < t_{SP}$  and it drops linearly with  $t$  during the snowplow phase for as long as  $k_B T_{soft} \gtrsim 6,000$  K, beyond which recombination takes place and the temperature drop stops.

The main difference between the scenario discussed above ( $\eta_s < 1$ ), and the one in which the radiation ahead of the shock deviates from thermal equilibrium, i.e.  $\eta_s > 1$ , is that absorption of the photons that carry most of the luminosity by unshocked electrons stops playing a role. This has two important implications. First, the energy of a single photon can significantly grow by IC over the shocked hot electrons without being absorbed. The limit on the observed energy of such IC upscattered photons is set by three factors: Compton losses at  $m_e c^2/\tau^2$ , escape time from the system and photoabsorption of extreme UV/soft X-rays by partially ionized pre-shock metals. Second, the coupling between the diffusing photons and unshocked electrons is done by Compton scattering only. This implies, in the parameter space that we consider, that the unshocked electrons and diffusing photons cannot maintain a single, well defined temperature. As

a result the photons produce a non trivial spectrum between the temperature of the unshocked electrons and  $m_e c^2/\tau^2$  and there may be no clear distinction between soft and hard components. Calculating the exact observed photon spectrum in that case is beyond the scope of this paper.

In general, our analysis of the soft component is not applicable anymore when the first of the following three takes place: (i) recombination becomes important, at which point  $T_{soft} \approx 6000$  K (ii) the hard component carries most of the luminosity (which always precedes the inapplicability of the diffusion approximation due to low wind optical depth) (iii)  $\eta_s > 1$ .

### 3.3.2. Hard component

The soft component is accompanied by harder photons, which can be generated by the hot electrons behind the shock in two ways, (i) free-free emission (ii) repeated IC upscatter of photons from the soft component. The total energy in IC upscattered photons is exponentially suppressed when  $\eta_s < 1$ , since only photons at the exponential tail of  $T_{soft}$  can be upscattered significantly before being absorbed by electrons with  $T_{soft}$ . It may be suppressed farther at  $T \gg T_{soft}$  by photoabsorption of partially ionized metals ahead of the shock. We therefore consider here only hot electrons' free-free emission. At breakout, the main cooling source of the hot electrons is IC of soft photons, yielding a free-free to IC emissivity ratio (c.f. Chevalier & Irwin 2012):

$$\frac{\epsilon_{ff,bo}}{\epsilon_{IC,bo}} = \frac{\alpha n_e (m_e c^2)^{3/2}}{4\sqrt{k_B T_e} \epsilon_{rad}} \approx 10^{-2} v_{bo,9}^{-2}, \quad (17)$$

where  $\epsilon_{rad} \approx \rho v^2/2$  at breakout. After the breakout, as long as  $\tau > 1$ ,

$$\frac{\epsilon_{ff}}{\epsilon_{IC}}(t) \propto \frac{1}{T^{1/2} v^3 \tau} \propto \begin{cases} t & t < t_{SP} \\ t^{2.5} & t > t_{SP} \end{cases}. \quad (18)$$

Therefore, IC remains the dominant cooling source for a long time after the breakout, suppressing the emission of hard photons. But even the hard photons that are emitted at  $T_e$  are not seen directly by the observer as long as the wind optical depth is significant. Compton losses during their diffusion towards the observer limit their energy to  $m_e c^2/\tau^2$  and farther reduces the luminosity of the hard component by a factor  $\tau^2 T_e/m_e c^2$  (Chevalier & Irwin 2012). Therefore, the observed temperature of the hard photons is

$$T_{hard}(t) = \min \left[ \frac{m_e c^2}{k_B \tau^2}, T_e(t) \right]. \quad (19)$$

The luminosity of hard photons, counting only contribution of free-free emission of the hot shocked electrons, is:

$$L_{hard}(t) \sim L(t) \frac{T_{hard}(t)}{T_e(t)} \min \left[ 1, \frac{\epsilon_{ff}}{\epsilon_{IC}}(t) \right]. \quad (20)$$

Equations 13, 17, 19 and  $\tau_{bo} = c/v_{bo}$  imply that when the breakout is at thermal equilibrium, this luminosity is always

$$L_{hard,bo} \sim 10^{-4} L_{bo}. \quad (21)$$

Equations 7 and 18 implies that at  $t < t_{SP}$ , while  $L_{\text{hard}} \ll L$ , it first evolves rapidly and then slows down, within the range :

$$L_{\text{hard}}(t < t_{SP}) \propto t^{2.5} \rightarrow t. \quad (22)$$

If the hard component is still subdominant during the transition to the snowplow phase, or if the breakout takes place during this phase, then its fraction out of the total luminosity rises quickly and multiplying this fraction with  $L(t)$ :

$$L_{\text{hard}}(t > t_{SP}) \propto t^3 \rightarrow t^{0.5}, \quad (23)$$

until it becomes comparable to the bolometric luminosity.

Finally, Equation 20 shows that right after breakout the hard photons from the hot electron's free-free emission carries only a tiny fraction ( $\sim 10^{-4}$ ) of the bolometric luminosity (which is seen in optical /UV). It implies, that even though the contribution of repeated IC scattering of  $T_{\text{soft}}$  photons is strongly suppressed, it may still dominate the luminosity of the hard component. Therefore, while  $\eta_s \ll 1$  implies,  $L_{\text{hard,bo}} \ll L_{\text{bo}}$ , the fraction may be higher than  $10^{-4}$  right after the breakout.

### 3.4. Criterion for fast cooling

We assumed above that the shocked plasma is cooling fast (within a dynamical time). Here we find when this assumption holds. A sufficient requirement for fast cooling is that free-free emission cools the hot electrons over a dynamical time. In case the Compton  $y$ -parameter drops below unity, it is also a necessary condition. The free-free cooling time at breakout is much shorter than the dynamical time for our considered range of  $v_{bo}$ :

$$\frac{t_{\text{cool,bo}}^{\text{ff}}}{t_{bo}} \approx \frac{1}{25} v_{bo,9}^4 T_{e,60}^{-1/2} \quad (24)$$

Past breakout, it evolves as

$$\frac{t_{\text{cool}}^{\text{ff}}}{t} \propto v^2 n_e^{-1} T_e^{-1/2} t^{-1} \propto \begin{cases} t^{0.6} & n = 12 \\ t^{0.2} & n = 7 \\ t^{-0.5} & n = 4 \end{cases} \quad (25)$$

Thus, if the shock is cooling fast at  $t_{SP}$  then it continues to cool fast also later. Requiring  $t_{\text{cool}}^{\text{ff}}(t_{SP})/t_{SP} < 1$  and taking  $t_{\text{cool}}^{\text{ff}}/t \propto t^{0.6}$  ( $n = 12$ ) all the way from breakout to  $t_{SP}$  shows that the shock enters the snowplow phase cooling fast as long as  $t_{bo} \gtrsim 6v_{bo,9}^{10/3} M_{10}^{3/4} E_{51}^{-1/4}$  d. This calculation over estimates the minimal  $t_{bo}$  in equation 25 by a factor of  $\sim 3$  since  $n$  varies from  $n \lesssim 12$  at breakout to  $n \approx 4$  at  $t_{SP}$ . Therefore, in the range of breakout velocities that we consider, the shock is always fast cooling for breakout times that are days or longer.

## 4. LIGHT CURVES OF THE DIFFERENT REGIMES

The light curve and spectral evolution depend on three time scales. The first two are  $t_{bo}$  and  $t_{SP}$ , which affect the hydrodynamics. The third timescale, which we denote  $t_{\text{hard}}$ , marks the time at which the hard component becomes the dominant one, thus affecting the spectral evolution. For breakout times of a day or longer, the order of appearance of these three characteristic timescales depends primarily on the breakout time  $t_{bo}$ .

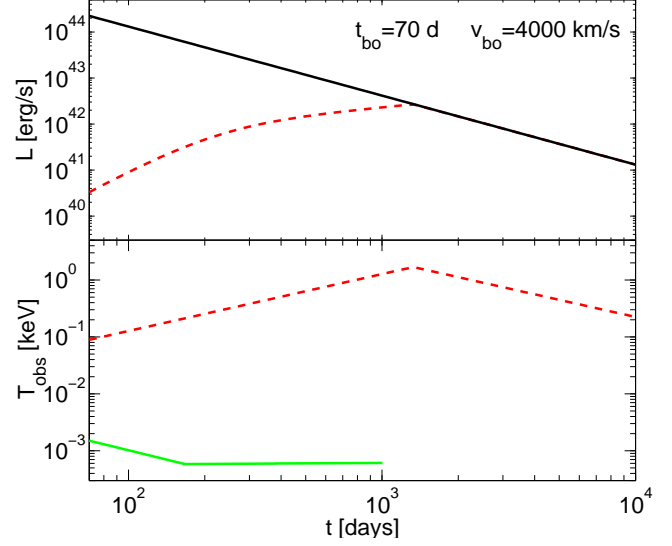


FIG. 2.— A breakout within the snowplow regime, with  $t_{bo} = 70$  d and  $v_{9,bo} = 0.4$  (matching  $E_{51} = 1.65$  and  $m_{bo} = 10M_{\odot}$ ), showing a very bright flash in the optical-UV, with a comparable rise time (not seen in the figure) and fall time. The temperature of the soft component (calculated for  $\kappa_{bf} \leq \kappa_{ff}$ ) and the bolometric luminosity (solid lines) decline as  $t^{-1.1}$  and  $t^{-1.5}$  respectively. Temperature decline stops around 6000 K, where recombination starts playing an important role. The luminosity of hard photons that are generated by free-free emission of the hot shocked electron and their temperature (dashed red lines) are strongly suppressed around the breakout (see text).  $\geq$  keV photons are observed only more than a year after the explosion. The breakout time and velocity are chosen to fit the observation of SN 2006gy.

Since at breakout the hard component is always a small fraction of the total luminosity,  $t_{bo} < t_{\text{hard}}$ , the evolution depends on the location of  $t_{SP}$  with respect to  $t_{bo}$  and  $t_{\text{hard}}$ . One regime is  $t_{SP} < t_{bo} < t_{\text{hard}}$ . The criterion for this regime was found in section 2. When  $t_{bo} < t_{SP}$ , there are two additional regimes, separated by the limiting case of  $t_{SP} = t_{\text{hard}}$ . In order to find the separating criterion we use Equation 20.  $t_{\text{hard}}$  is the earliest time that satisfies  $L_{\text{hard}} \approx L$ , namely that both  $\tau^2 \approx m_e c^2 / k_B T_e$  and  $\epsilon^{\text{ff}} \approx \epsilon^{\text{IC}}$  are satisfied. Setting  $t_{SP} = t_{\text{hard}}$  the condition  $\tau^2 \approx m_e c^2 / k_B T_e$ , which is the last to be satisfied for typical parameters, implies  $\tau \approx 5E_{51}^{1/2} M_{10}^{-1/2}$ , where we used  $v(t_{SP}) \approx \sqrt{2E/M_{ej}}$  and Equation 13. Using Equation 5 and setting  $\tau = 5E_{51}^{1/2} M_{10}^{-1/2}$  one finds that  $t_{SP} = t_{\text{hard}}$  when  $t_{bo,d} \approx 20M_{10}^{0.75} E_{51}^{-0.25}$ . We thus obtain the following three regimes with respect to  $t_{SP}$ :

$$\begin{aligned} t_{SP} < t_{bo} & \quad t_{bo,d} \gtrsim 80M_{10}^{0.75} E_{51}^{-0.25} \\ t_{bo} < t_{SP} < t_{\text{hard}} & \quad 20M_{10}^{0.75} E_{51}^{-0.25} \lesssim t_{bo,d} \lesssim 80M_{10}^{0.75} E_{51}^{-0.25} \\ t_{bo} < t_{\text{hard}} < t_{SP} & \quad 1 \lesssim t_{bo,d} < 20M_{10}^{0.75} E_{51}^{-0.25} \end{aligned} \quad (26)$$

These regimes roughly match initial (breakout)  $n$  values of 4, 7 and 12, respectively. Below we discuss the luminosity and spectral evolution in each of these regimes.

### 4.1. Late breakout ( $t_{SP} < t_{bo}$ )

$$t_{bo,d} \gtrsim 80M_{10}^{0.75} E_{51}^{-0.25}$$

If the progenitor went through an extreme mass loss episode just prior to the explosion, the mass in the wind

can be larger than the ejecta mass. In such a scenario the breakout may take place weeks to months after the explosion, near the time that, or even after, the reverse shock is exhausted. The entire explosion energy is released then around  $t_{bo}$ . If the ejecta is several solar masses with  $\sim 10^{51}$  erg, the breakout velocity is  $3000 - 5000 \text{ km s}^{-1}$ . At these velocities  $\eta_s < 1$  throughout the evolution even for  $\kappa_{bf} \leq \kappa_{ff}$ , implying a very bright optical-UV flash, with a comparable rise time and fall time, and a typical temperature of  $\sim 1 - 5 \times 10^4 \text{ K}$ . Following breakout, the luminosity and temperature of the soft component decline as  $t^{-1.5}$  and  $t^{-1.1}$  respectively. The temperature decline stops around 6000 K, where recombination starts playing an important role. The breakout free-free hard component is strongly suppressed, ( $\sim 10^{-4}$  of the total luminosity) by the IC cooling dominance and the high wind optical depth. Contribution of IC photons to the hard component may dominate over free-free at early time, but since  $\eta_s \ll 1$  their luminosity will still be much lower than  $L_{bol}$ . Moreover, the temperature of hard photons is limited during the breakout to  $\lesssim 0.1 \text{ keV}$  by Compton losses during the diffusion through the unshocked wind (Chevalier & Irwin 2012). The hardness and luminosity of the hard component rise following the breakout, but a significant emission above 1 keV starts only at  $\sim 10t_{bo}$ . Luminous hard X-ray emission is expected in this regime only if the breakout velocity is high, which requires either a low ejecta mass  $\sim M_\odot$  or a very high energy explosion  $\sim 10^{52}$  erg. Figure 2 depicts the luminosity and temperature evolution of a breakout near the snowplow phase with  $t_{bo} = 70 \text{ d}$  and  $v_{9,bo} = 0.4$  where the evolution discussed above is seen. The breakout time scale and velocity fit the observations of SN 2006gy (Ofek et al. 2007; Smith et al. 2007), which was suggested by Chevalier & Irwin (2011) to be a shock breakout through a wind. The luminosity and temperature of the dominating soft component of SN 2006gy are recovered with these  $t_{bo}$  and  $v_{bo}$ . Similarly to the conclusion of Chevalier & Irwin (2012), we find a strongly suppressed X-ray luminosity, with keV photons appearing only years after the explosion (assuming that the shock does not encounter the edge of the wind at an earlier time).

Note that already during the breakout the mass of the wind is comparable to the mass of the ejecta, and the mass accumulated by the shock grows as  $t^{1/2}$ . Therefore, if the wind mass is not much larger than the ejecta mass, the shock encounters the end of the massive wind not too long after  $t_{bo}$ .

#### 4.2. Early breakout, ( $t_{bo} < t_{hard} < t_{SP}$ )

$$1 \lesssim t_{bo,d} \lesssim 20 M_{10}^{0.75} E_{51}^{-0.25}$$

If breakout occurs early the shock velocity is larger, ranging from  $5,000\text{-}10,000 \text{ km s}^{-1}$  for typical SNe. For low metallicity, i.e.  $\kappa_{bf} \leq \kappa_{ff}$ , the breakout emission is at a marginal thermal equilibrium and a breakout temperature in the range  $10^4 - 10^6 \text{ K}$  is expected for SNe with typical energy and ejecta mass. Figure 3 depicts the luminosity and temperature of the soft and hard components in a breakout with  $t_{bo} = 10 \text{ d}$  and  $v_{bo} = 5,000 \text{ km s}^{-1}$ . If metallicity is low, the soft component is in marginal thermal equilibrium during breakout,  $\eta_{bo} = 0.3$ , resulting in  $T_{bo,obs} \approx 25,000 \text{ K}$ . Following the breakout

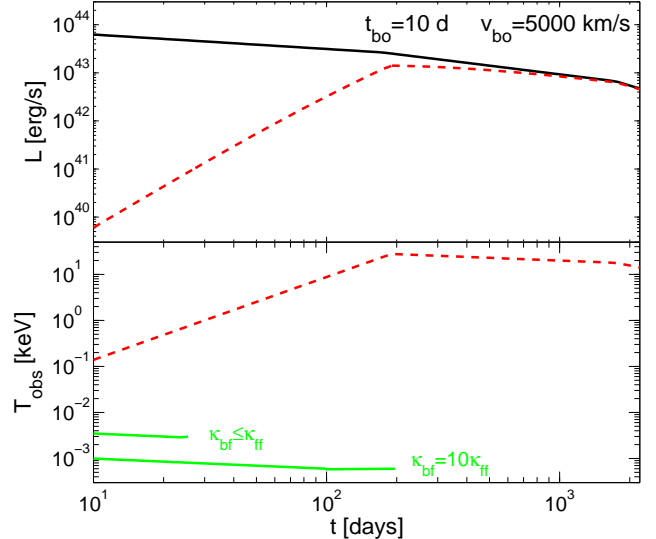


FIG. 3.— Early breakout of  $t_{bo} = 10 \text{ d}$  and  $v_{bo} = 5,000 \text{ km s}^{-1}$ , where  $t_{SP}$  is calculated for  $E_{51} = 1$  and  $M_{10} = 1.25$ . The Bolometric luminosity and soft component temperature are marked with *solid lines*. The temporal decay of the bolometric luminosity is shifted from  $t^{-0.3}$  ( $n=12$ ) to  $t^{-0.6}$  ( $n=7$ ) at  $0.1t_{SP}$ , to account for the flattening of the ejecta profile once  $m$  approaches  $M_{ej}$ . Such a breakout may explain SNe like PTF 09uj (Ofek et al. 2010).  $T_{soft}$  is plotted for two different absorption opacities. When  $\kappa_{bf} \leq \kappa_{ff}$  (low metallicity) then  $\eta_{bo} = 0.3$  and  $T_{soft}$  decreases slowly before thermal equilibrium is broken at day 25 (where we stop following it). In case that  $\kappa_{bf} = 10\kappa_{ff}$  (higher metallicity) then  $\eta_{bo} = 0.03$  and  $T_{soft}$  remains in thermal equilibrium until the soft component becomes negligible. The luminosity and temperature of the hard photons are marked with *dashed lines*. The luminosity includes only contribution from hot shocked electrons' free-free emission, which is very faint at first, and becomes brighter and harder quickly to dominate the flux from day 200 and on. Contribution from IC photons (not included in the hard component here) may be important at early time, especially in case that  $\kappa_{bf} \leq \kappa_{ff}$  where thermal equilibrium is marginal. This may result in significant X-ray emission also earlier than day 200. Such events make excellent candidates for X-ray searches  $\sim 100\text{-}300 \text{ d}$  after the SN explosion and possibly even earlier.

$\eta_s$  increases roughly linearly with time, implying that it becomes harder for the radiation to maintain thermal equilibrium. As a result  $T_{soft}$  declines very slowly until day 25, when thermal equilibrium cannot be maintained anymore. If  $\kappa_{bf} = 10\kappa_{ff}$ , then  $\eta_{bo} = 0.03$  and  $T_{soft}$  remains in thermal equilibrium until the soft component becomes negligible. In that case  $T_{bo,obs} \approx 10,000 \text{ K}$ , and  $T_{soft}$  decreases slowly after breakout towards recombination temperature. Hard photons from free-free emission carry a very small fraction of the bolometric luminosity at first (only  $\sim 10^{-4}$ ), and thus hard IC photons may dominate the hard component at early times (especially when  $\kappa_{bf} \leq \kappa_{ff}$  and the thermal coupling is weak). The temperature of hard photons is limited after breakout to  $\sim 0.5 \text{ keV}$ . The hard component becomes brighter and harder quickly, with hard X-rays and soft gamma-rays dominating the flux after 200 days (and possibly earlier if IC produces hard photons efficiently when  $\eta_s > 1$ ). Since the luminosity decays slowly before  $t_{SP}$ , these events are good candidates for X-ray searches  $\sim 100\text{-}300$  day after the SN explosion, when  $> \text{keV}$  photons must dominate the luminosity and before the snowplow phase starts. Finally, the luminosity increases with breakout time. Therefore, breakouts with larger  $t_{bo}$  (which are



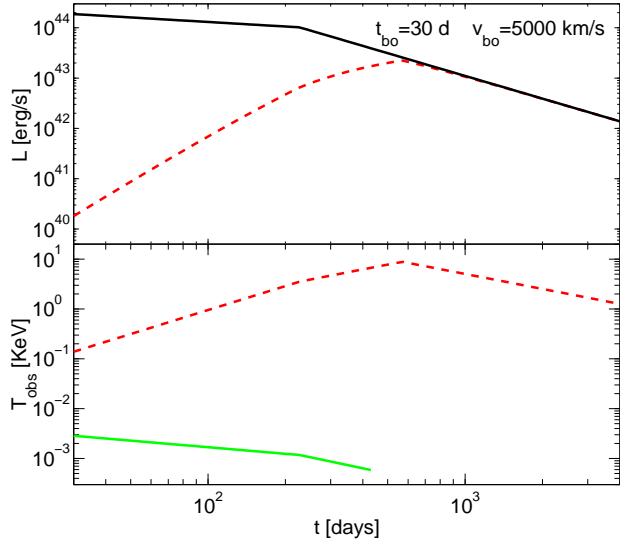


FIG. 4.— An intermediate regime breakout, of  $t_{bo} = 30$  d and  $v_{bo} = 5,000$  km s $^{-1}$ .  $t_{SP}$  is calculated for  $E_{51} = 1$  and  $M_{10} = 1$  and  $T_{soft}$  calculated for  $\kappa_{bf} \leq \kappa_{ff}$ . The transition to the snowplow phase happens at day  $\approx 230$ , while the hard component gains dominance only after this transition, reaching a lower luminosity and softer X-ray temperatures compared to those of the early regime. If the breakout is early enough, so that  $t_{hard} \sim t_{SP}$ , such events produce the brightest X-ray luminosity among all the cases. Notations are similar to figures 2 and 3.

still in this regime) produce brighter X-ray events.

Early breakout may explain SN PTF 09uj, as suggested by Ofek et al. (2010). The breakout temperature and luminosity of the case depicted in figure 3 are consistent with the observations (Ofek et al. 2010).

#### 4.3. Intermediate breakout time, ( $t_{bo} < t_{SP} < t_{hard}$ )

$$20M_{10}^{0.75}E_{51}^{-0.25} \lesssim t_{bo,d} \lesssim 80M_{10}^{0.75}E_{51}^{-0.25}$$

Figure 4 presents the luminosity and temperature of an intermediate case, where the breakout takes place before the transition to the snowplow phase, but the hard component may become dominant only after this transition. The properties of the breakout and the emission that follows soon after it are similar to those described in the early breakout case. The main difference from the early breakout case is that the hard component may not dominate the luminosity at  $t_{SP}$  and by the time that it does, the luminosity may already be dropping fast. If the breakout is early enough and  $t_{hard} \sim t_{SP}$ , then the X-ray luminosity must be high. In fact these events produce the brightest X-ray luminosity among all the cases discussed in this paper.

## 5. SUMMARY

We examine the emission from a shock breakout through a thick wind. We restrict our exploration to breakout time scales that are days or longer, which are easier to detect, and velocities in the range 3,000-15,000 km s $^{-1}$ , as expected for typical SNe. We further restrict our focus to cases where thermal equilibrium prevails during the evolution of the collisionless shock. For low metallicities this restriction reduces the shock velocities of interest to the lower part of the above range. We consider a standard wind profile  $\rho_w \propto r^{-2}$ , that is extended

beyond the breakout radius. Following the breakout, the internal energy in these systems is dominated by the wind material that is heated by the forward shock (Chevalier & Irwin 2011; Balberg & Loeb 2011), which makes a transition from a radiation mediated shock to a collisionless shock at the breakout (Katz et al. 2011b). Our main conclusions are listed below.

(i) The breakout and following emission are very luminous. In the regime that we explore, the shocked plasma is always cooling fast (see the exact condition in section 3.4), converting all the shock luminosity into radiation. Therefore, if the wind mass is comparable to, or larger than, the ejecta mass, then all the SN kinetic energy is radiated away. If the wind mass,  $M_w$  is smaller than  $M_{ej}$  then the energy radiated during the interaction is  $\sim EM_w/M_{ej}$ . This result supports the suggestion by Chevalier & Irwin (2011) that at least some ultra-luminous type IIIn SNe are such breakouts.

(ii) As long as photons that diffuse ahead of the shock maintain thermal equilibrium with the unshocked gas, the post-breakout emission is composed of two spectral components - soft and hard. The electrons behind the collisionless shock are heated to temperatures of  $\sim \min[60, 200v_9^2]$  keV (Katz et al. 2011b). The soft component is generated by the unshocked gas ahead of the shock, while the hard component is generated by the hot shocked electrons via free-free emission and IC of a small fraction of the soft photons.

(iii) The soft component may or may not be in thermal equilibrium during the breakout, even in the narrow velocity range of 3,000-15,000 km s $^{-1}$ . Thermal equilibrium is expected for all slower breakouts  $\lesssim 7,000$  km s $^{-1}$ , and also for faster breakouts if there is a significant bound-free absorption (i.e., high metallicity). The breakout is then bright in optical/UV, with a temperature of  $10^4 - 10^5$  K. In faster shocks that are out of thermal equilibrium the breakout temperature can be as high as  $5 \times 10^6$  K. In that case, the breakout X-rays can be much brighter than the optical/UV.

(iv) If thermal equilibrium is maintained ahead of the shock the hard component is suppressed as long as IC cooling is more efficient than free-free cooling (Chevalier & Irwin 2012). In that case hard photons from free-free emission of hot electrons behind the forward shock carry at the breakout only  $\sim 10^{-4}$  of the soft component energy. The luminosity of hard photons from IC over the same electrons may be higher, but it is also a small fraction of the bolometric luminosity. The hard component luminosity rises quickly after breakout. It becomes dominant at  $\sim 10 - 50t_{bo}$ .

(v) The temperature of the hard component is  $m_e c^2/\tau^2$ , which at breakout is 0.1–1 keV. It rises as  $t^2$  after breakouts with  $t_{bo} \lesssim 80$  d and as  $t$  for longer breakouts.

The post-breakout evolution can be divided into three regimes according to the breakout time. (i) Late breakouts (typically  $t_{bo} > 80$  d) are very bright in optical/UV and for typical parameters are very dim in X-rays at early time.  $\sim 1$  keV X-rays peak around  $20t_{bo}$ , carrying only  $\sim 10^{-2}$  of the breakout energy. (ii) Early breakout (typically  $1 < t_{bo} < 20$  d) bolometric luminosity is lower and it can be either in or out of thermal equilibrium for typical parameters. If it is out of thermal equilibrium the

emission can be bright in X-rays soon after the breakout (and possibly dim in optical/UV). If it is in thermal equilibrium then X-rays are suppressed after the breakout, but their luminosity and hardness rises quickly to gain dominance, at most at  $t \sim 20t_{bo}$ . (iii) Intermediate breakouts (typically  $20 \text{ d} < t_{bo} < 80 \text{ d}$ ) are typically in thermal equilibrium and are therefore bright in optical/UV while X-ray emission is suppressed at breakout. But,  $\sim 1 - 10 \text{ keV}$  X-rays become dominant at most at  $t \sim 20t_{bo}$  with a luminosity that may be almost as high as that of the breakout pulse.

In our calculations we ignore the radius at which the thick wind ends. Once the wind density drops abruptly the forward shock becomes inefficient and the luminosity fades quickly (Chevalier & Irwin 2011). Since the mass of the progenitor at birth is limited, and the mass in the wind needed for an extended breakout is considerable, it is expected that the light curves we present will be terminated at some point. For example, in order for the light curve to remain bright until  $t_{SP}$  the wind mass must be  $\gtrsim M_{ej}$ . Even when  $M_w > M_{ej}$  the collected mass is  $\propto t^{1/2}$  after  $t_{SP}$ , limiting the lifetime of the bright emission. In terms of the prospects of observing X-rays, this consideration makes earlier breakouts more attractive, since the mass that early breakout events collect by the time that the hard component dominates is lower.

We do not address the extinction of soft X-rays due to photoabsorption by partially ionized unshocked wind (Chevalier & Irwin 2012). This process may suppress softer-end photons of the hard component as well as hard

photons of the soft component, if the latter is far from thermal equilibrium. If photoabsorption is important then the observed flux of soft X-rays is lower than the one that we predict.

Finally, our treatment ignores the contribution of emission from ejecta mass before it is shocked by the reverse shock. Once the optical depth of the wind drops, this emission becomes similar to the emission from a typical SN without a thick wind (e.g., typical IIP, Ib and Ic SNe). The emission from the forward shock that we consider here always outshines this emission (in terms of bolometric luminosity). But, at late times, when most of the forward shock emission is in hard photons, the contribution from inner layers may dominate the IR-optical emission.

To conclude, breakouts through thick winds produce very bright SNe with a potential for detection across the entire electromagnetic spectrum. The brightest phase is the breakout, which is typically dominated by optical-UV emission. In that case early X-ray emission is suppressed, but X-rays becomes harder and their luminosity rises quickly after the breakout, peaking at most after  $\sim 10 - 50 t_{bo}$ .

We thank Eran Ofek and Boaz Katz for helpful discussions and comments, and the anonymous referee for further helpful comments. G.S. and E.N. were partially supported by an ISF grant (174/08) and by an ERC starting grant (GRB-SN 279369). R.S. was partially supported by ERC and IRG grants, and a Packard Fellowships.

#### REFERENCES

- Arcavi, I., et al. 2011, *ApJL*, 742, L18  
 Balberg, S., & Loeb, A. 2011, *MNRAS*, 414, 1715  
 Campana, S., et al. 2006, *Nature*, 442, 1008  
 Chevalier, R. A. 1982, *ApJ*, 258, 790  
 Chevalier, R. A., & Fransson, C. 2008, *ApJL*, 683, L135  
 Chevalier, R. A., & Irwin, C. M. 2011, *ApJL*, 729, L6+  
 —. 2012, *ApJL*, 747, L17  
 Colgate, S. A. 1974, *ApJ*, 187, 333  
 Couch, S. M., Pooley, D., Wheeler, J. C., & Milosavljević, M. 2011, *ApJ*, 727, 104  
 Ensmann, L., & Burrows, A. 1992, *ApJ*, 393, 742  
 Falk, S. W. 1978, *ApJL*, 225, L133  
 Gezari, S., et al. 2008, *ApJL*, 683, L131  
 —. 2010, *ApJL*, 720, L77  
 Imshennik, V. S., Nadezhin, D. K., & Utrobin, V. P. 1981, *Ap&SS*, 78, 105  
 Katz, B., Budnik, R., & Waxman, E. 2010, *ApJ*, 716, 781  
 Katz, B., Sapir, N., & Waxman, E. 2011a, *ArXiv e-prints*  
 —. 2011b, *ArXiv e-prints*  
 Klein, R. I., & Chevalier, R. A. 1978, *ApJL*, 223, L109  
 Matzner, C. D., & McKee, C. F. 1999, *ApJ*, 510, 379  
 Modjaz, M., et al. 2009, *ApJ*, 702, 226  
 Moriya, T. J., & Tominaga, N. 2011, *ArXiv e-prints*  
 Murase, K., Thompson, T. A., Lacki, B. C., & Beacom, J. F. 2011, *Phys. Rev. D*, 84, 043003  
 Nakar, E., & Sari, R. 2010, *ApJ*, 725, 904  
 —. 2011, *ArXiv e-prints*  
 Ofek, E. O., et al. 2007, *ApJL*, 659, L13  
 —. 2010, *ApJ*, 724, 1396  
 Piro, A. L., Chang, P., & Weinberg, N. N. 2010, *ApJ*, 708, 598  
 Rabinak, I., & Waxman, E. 2011, *ApJ*, 728, 63  
 Sakurai, A. 1960, *Communications on Pure and Applied Mathematics*, 13, 353  
 Schawinski, K., et al. 2008, *Science*, 321, 223  
 Smith, N., et al. 2007, *ApJ*, 666, 1116  
 Soderberg, A. M., et al. 2008, *Nature*, 453, 469  
 Weaver, T. A. 1976, *ApJS*, 32, 233